Appl. Phys. A (2015) 120:1537–1543
DOI 10.1007/s00339-015-9353-3

Applied Physics A
Materials Science & Processing

# Conductivity study and correlated barrier hopping (CBH) conduction mechanism in diphosphate compound

Y. Ben Taher[1] · A. Oueslati[1] · N. K. Maaloul[2] · K. Khirouni[2] · M. Gargouri[1]

Received: 27 June 2015 / Accepted: 7 July 2015 / Published online: 29 July 2015


**Abstract** In this paper, we report some physical properties of $AgAlP_2O_7$ compound obtained through the standard solid-state reaction technique. $AgAlP_2O_7$ has been studied by X-ray diffraction, Raman spectroscopy and impedance spectroscopy. The title compound crystallized at room temperature ($T = 300$ K) in the monoclinic system with $P2_{1/c}$ space group. The electrical properties were studied over a wide range of temperature (440–640 K) in the frequency range of 40 Hz–10 MHz. Study of frequency dependence of AC conductivity suggests that the material obeys the Jonscher's universal dynamic law. The conductivity is equal to $9.37 \times 10^{-5}\ \Omega\ cm^{-1}$ at 640 K, and it is thermally activated with activation energy of 0.76 eV. The variation of DC conductivity with temperature follows the Arrhenius behavior. The calculated values of $s$ decreased with temperature. This behavior reveals that the conduction mechanism is correlated with barrier hopping. The binding energy $W_m$ and the hopping distance $R_\omega$ were deduced.

## 1 Introduction

Diphosphates, often also called pyrophosphates, constitute the largest family of condensed phosphates, and a great number of compounds of different stoichiometries, containing a single or different types of cations, are prepared [1]. They are the subject of various research works throughout the world. Some of them are used for their acid–base properties or for their oxidizing character. They can be used as a nonlinear optic materials, high-temperature ionic conductors, solid electrolytes for high-energy density batteries, ion exchange materials and catalysts [2, 9]. Extensive research work has been made in these diphosphate compounds like $KAlP_2O_7$, $CsAlP_2O_7$, $NaInP_2O_7$, and this interesting field has been grown due to the important characterization such as optical characterization [10]. Recent works were published during last two years on diphosphate materials such as $KAlP_2O_7$, $NaAlP_2O_7$ and $AgFeP_2O_7$ [11, 13].

In fact, the study of diphosphates has become more popular particularly after the development of NASICON and LISICON groups of fast ionic conductors [14, 15].

Compositions with general formula $A^IB^{III}P_2O_7$ containing simultaneously an alkaline ion ($A^+$ = Na, K, Li, …) and a trivalent cation ($B^{3+}$ = Fe, Al, Cr, …) are an important materials, mainly due to their prospective potential technological applications and their highest conductivity [16, 17].

Among these compounds, $AgAlP_2O_7$ is isotypic with $NaFeP_2O_7$-II [18], and it is one of the monoclinic systems with the space group $P2_{1/c}$. The structure (Fig. 1) containing $AlO_6$ octahedra and the $[P_2O_7]^{4-}$ anion consists of a pair $PO_4$ tetrahedra. The electric study carried out on phosphate materials is scarce with respect to two different aspects: measurements under continuous mode and under alternative mode. The measurements of AC conductivity have been widely used to understand the conduction process in materials. Different models are based on the relaxation caused by the hopping or tunneling of electrons or atoms between equilibrium sites.

✉ Y. Ben Taher
youssef.btaher@yahoo.fr

[1] Condensed Matter Laboratory, Faculty of Sciences, University of Sfax, B.P. 1171, 3000 Sfax, Tunisia

[2] Laboratoire de Physique des Matériaux et des Nanomatériaux Appliquée à l'Environnement, Faculté des Sciences de Gabès, Gabès, Tunisia

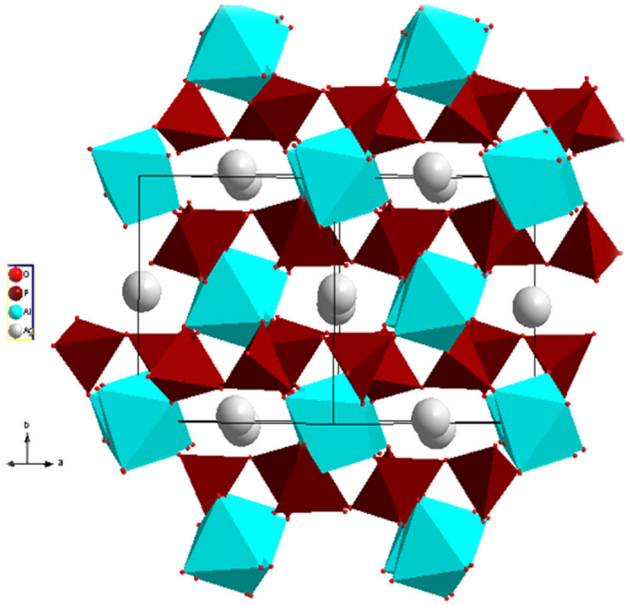

**Fig. 1** Crystal structure of $AgAlP_2O_7$

The main objective of this paper is to present and discuss the electrical properties of $AgAlP_2O_7$ compound as a function of frequency and temperature.

## 2 Experimental

The $AgAlP_2O_7$ compound has been prepared using the standard solid-state reaction techniques. The starting materials were $Ag_2CO_3$, $Al_2O_3$ and $NH_4H_2PO_4$ with purity 99.99 %. These materials were ground, mixed and progressively heated from room temperature to 573 K at first step in order to expel $NH_3$, $H_2O$ and $CO_2$. The calcined powder was heated once at 1073 K for 8 h.

X-ray powder diffraction pattern was recorded using a Philips PW 1710 diffractometer operating with copper radiation $K_\alpha = 1.5418$ Å. Unit cell parameters of the synthesized compound have been refined by the least-square method from the powder data. Raman scattering investigation was performed on powder, using a spectrometer type Horiba Jobin–Yvon T64000.

A pellet with a diameter of 8 mm and thickness of about 1.2 mm using 3 T/cm$^2$ uniaxial pressure was used for electrical conductivity. The measurements were performed using an Agilent 4294A impedance analyzer (two platinum electrodes and we use an evaporation sputtering). The temperature range was between 440 and 640 K.

## 3 Results and discussion

### 3.1 X-ray powder diffraction

The X-ray powder diffraction was performed at room temperature on powder finely ground in an agate mortar with $CuK_\alpha$ radiation and $2\theta$ range from 10° to 60°. All the reflection peaks were indexed in the monoclinic system with $P2_{1/c}$ space group. These refined lattice parameters are: $a = 7.332(4)$Å, $b = 7.904(3)$Å, $c = 9.513(3)$Å, and $\alpha = 111.830(5)°$. These values are in good agreement with the literature [18].

### 3.2 Raman spectroscopy

The Raman spectrum of the $AgAlP_2O_7$ compound at room temperature is shown in Fig. 2. It reveals different peaks which can be attributed according to published results [19–21] in similar compound.

The peaks due to the symmetric and asymmetric stretching frequencies of $PO_3$ in $P_2O_7^{4-}$ are generally observed in the regions 994–1209 cm$^{-1}$. The bands observed in the regions 861–960 and 600–743 cm$^{-1}$ are attributed to the asymmetric and symmetric P–O–P stretching modes. The bands due to the symmetric and asymmetric binding vibrations of $PO_3$ are generally observed in the regions 200–575 cm$^{-1}$. Band assignments for the fundamental modes of $P_2O_7^{4-}$ anions are listed in Table 1.

### 3.3 Impedance analysis and equivalent circuit

The complex impedance analysis technique is based on analyzing the AC response of a system to a sinusoidal

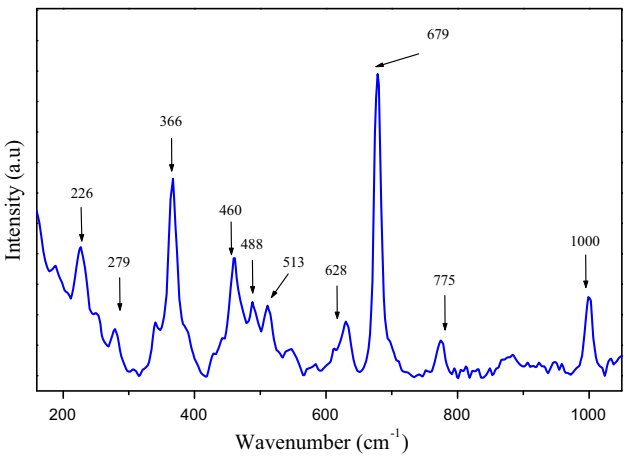


**Fig. 2** Raman spectrum and peak position of $NaAlP_2O_7$

**Table 1** Observed Raman frequencies for $AgAlP_2O_7$

| Bands ($cm^{-1}$) | Assignment |
|---|---|
| 1000 | $\upsilon_{as}$ $PO_3$ |
| 775, 679, 628 | $\upsilon_{as}$ P–O–P, $\upsilon_s$ P–O–P |
| 513, 488, 460, 366, 279, 226 | $\delta$ $PO_3$ |

perturbation and subsequent calculation of impedance as a function of the frequency of the perturbation. The technique can be used for electrical characterization of polycrystalline materials [22]. To understand the contribution of grain and electrode effects observed in structural characterization, we compute from experimental data real $Z'$ and imaginary $Z''$ parts of the impedance and we plot $Z''$ versus $Z'$.

The complex impedance spectra ($Z''$ vs. $Z'$) of the $AgAlP_2O_7$ compound at several temperatures are presented in Fig. 3a–c. The center of this semicircle is depressed below the real axis, which indicates a non-Debye type of relaxation [23]. The lower frequency response corresponds to the electrode processes and the higher one to the bulk effects.

To interpret such a diagram, it is necessary to modelize the sample. At higher frequencies, the observed shapes are typical of relaxation mechanisms modelized by a circuit constituted by a resistor $R_g$ in parallel with a constant-phase element $CPE_g$. At lower frequencies, electrode polarization effects transduced by constant-phase element ($CPE_e$) are evidenced (inset Fig. 3).

In order to justify the choice of equivalent circuit, we present in Fig. 4 the experimental and calculated $Z''$ values at different temperature, using the parameters of the equivalent circuit model. The good conformity between the experimental and calculated data indicates that the equivalent circuit describes the compound–electrode interface reasonably well.

Figure 5 shows the variation of imaginary part of impedance ($Z''$) with angular frequency for some representative temperatures. The spectra are characterized by appearance of peaks, which shift to higher frequencies with increasing temperature. The broadening of peaks in frequency suggests that there is a spread of relaxation times. The merger of $Z''$ values in the high-frequency region may possibly be an indication of the accumulation of space charge in the material [24].

The obtained fitted values of $R_g$, $CPE_g$ and $CPE_e$ for different temperatures are summarized in Table 2. We can see that the value of grain resistance ($R_g$) decreases with the increase in temperature. In addition, the value of conductivity increases with the increase in temperature, due to the charge carriers according to the hopping conduction mechanism [25].

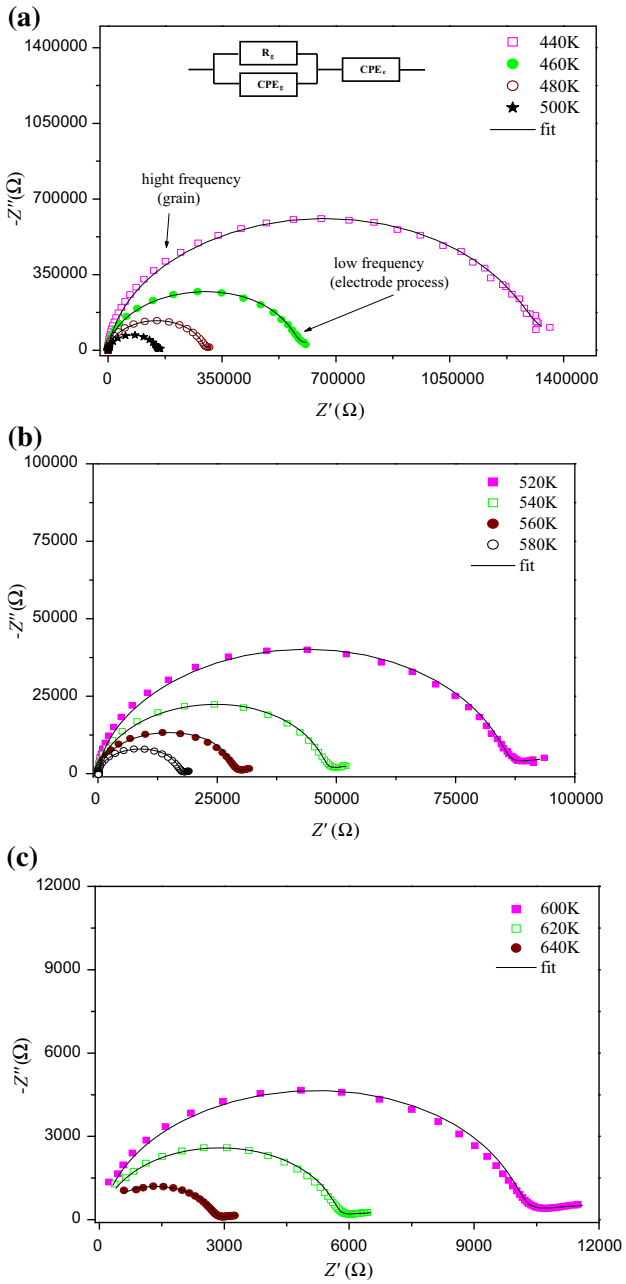


**Fig. 3** Experimental and calculated Nyquist plots at different temperature: (**a**) from 440 to 500 K temperature range, (**b**) from 520 to 550 K temperature range, (**c**) from 600 to 640 K temperature range. The equivalent circuit model is shown in the inset

The values of capacitance ($Q_g$) are in the range of pico-farad, implying that the single semicircle response is from grain interiors. The values of capacitance electrode $Q_e$ are in the range of micro-farad implying the electrode effect in low frequency.

The frequency $\omega_{max}$ corresponding to $Z''_{max}$ gives the most probable relaxation time $\tau_m$ from the condition $\omega_{max}\tau_m = 1$. Figure 6 shows a plot of the ($\ln \omega_{max}$) versus 1000/T. It follows Arrhenius relation. The dots are the

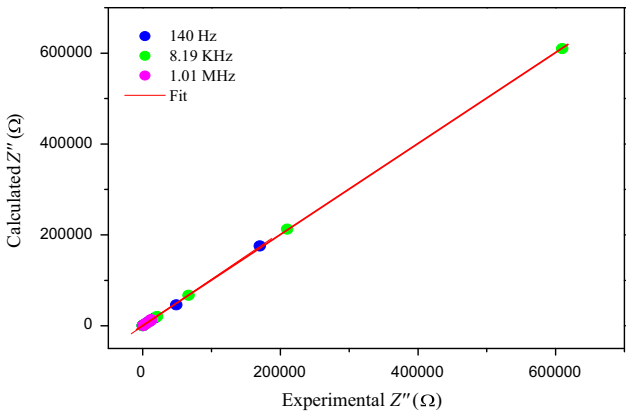


**Fig. 4** Correlation graphics between $Z''$ calculated and $Z''$ experimental

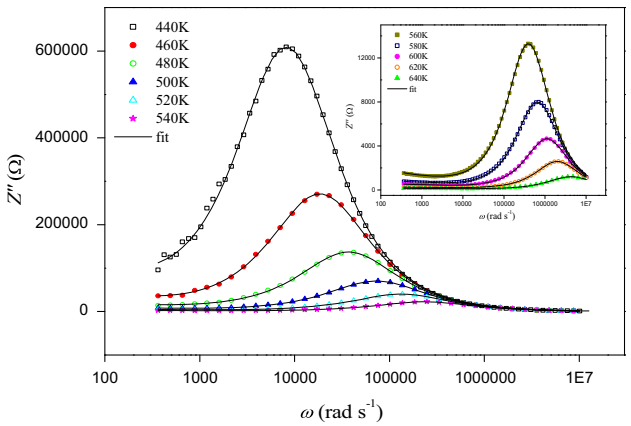


**Fig. 5** Experimental and calculated imaginary parts of impedance at different temperatures, inset high-temperature range

**Table 2** Equivalent circuit parameters for the $AgAlP_2O_7$ compound

| $T$(K) | $R_g$ (KΩ) | $Q_g$ ($10^{-11}$ F) | $\alpha_g$ | $Q_e$ ($10^{-7}$ F) | $\alpha_e$ |
|---|---|---|---|---|---|
| 440 | 1290 | 14.4 | 0.953 | 2.33 | 0.74 |
| 460 | 573 | 13.9 | 0.959 | 2.10 | 0.79 |
| 480 | 289 | 14.3 | 0.958 | 9.64 | 0.78 |
| 500 | 149 | 15.2 | 0.954 | 8.37 | 0.75 |
| 520 | 84.9 | 15.2 | 0.956 | 9.26 | 0.76 |
| 540 | 46.8 | 14.5 | 0.962 | 8.23 | 0.69 |
| 560 | 27.9 | 15.3 | 0.960 | 8.22 | 0.64 |
| 580 | 16.8 | 16.2 | 0.957 | 7.15 | 0.61 |
| 600 | 9.78 | 17.1 | 0.956 | 7.70 | 0.66 |
| 620 | 5.48 | 19.3 | 0.950 | 9.56 | 0.62 |
| 640 | 2.59 | 32.7 | 0.920 | 9.45 | 0.67 |

experimental data, and the solid line is the least-squares straight-line fit. The activation energy calculated from this figure is 0.76 eV.

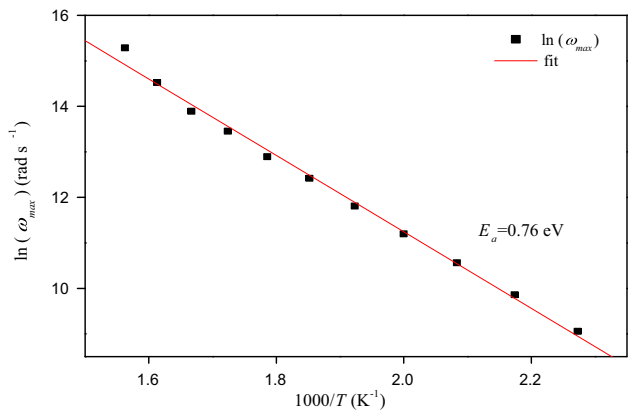


**Fig. 6** Temperature dependence of the relaxation frequency obtained from the impedance measurement

Figure 7 shows the plot of the impedance $Z''$ at different temperatures, where frequency axis is normalized by $\omega_{max}$ and $Z''$ axis by $Z''_{max}$ at various temperatures. The normalized plot shows that all the curves overlap on a single master curve. This indicates that all possible relaxation mechanisms occurring at different frequencies exhibit the same thermal energy and the dynamical processes are temperature independent.

The value of grain conductivity of the material was evaluated using the relation: $\sigma_g = \frac{e}{R_g * S}$, where $R_g$ is the bulk resistance, e is the thickness, and s is the surface of the sample. Figure 8 shows an increase in the DC conductivity with a rise in temperature. This behavior can be explained by thermally activated transport processes governed by an Arrhenius relation $\sigma_g T = B \exp\left(\frac{-E_a}{K_b T}\right)$, where $B$ is the pre-exponential factor and $E_a = 0.76$ eV is the activation energy of mobile charge carrier. The $AgAlP_2O_7$ compounds crystallize in the monoclinic system with P21/c space group; in this structure, the $Ag^+$ ions are located in

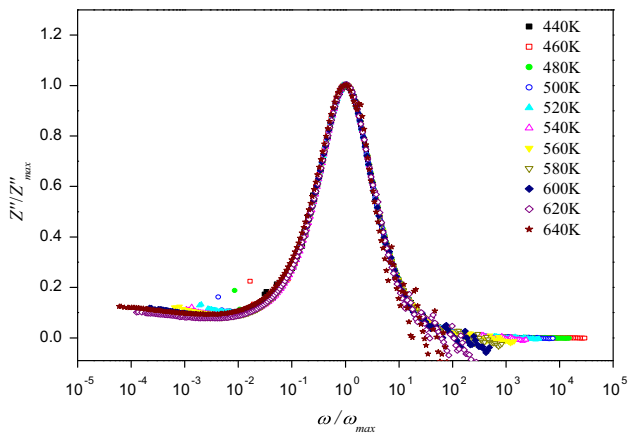


**Fig. 7** Scaling behavior of $Z''$ at various temperatures

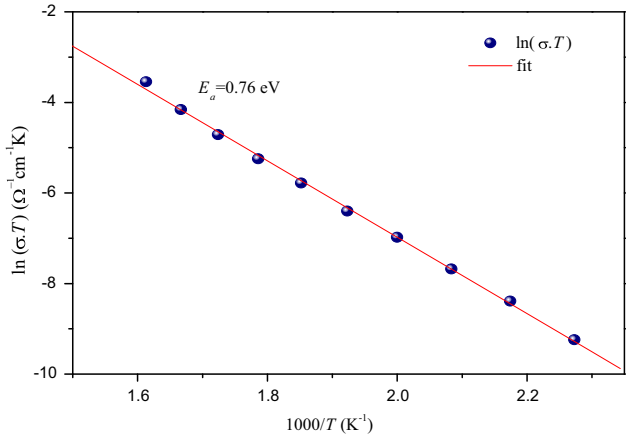


**Fig. 8** Temperature dependence of grain conductivity $\sigma_g$

tunnels formed by $P_2O_7$ polyhedra and $AlO_6$ octahedra. In short, this suggests that the conduction in this material is due to the motion of the $Ag^+$ ions along [101] tunnels' direction presented in the structure of the investigated material. The values of the activation energy calculated from conductivity and obtained from the relaxation in $Z''$ are very close: This improves that the relaxation process and the electrical conductivity are ascribed to the same effect.

### 3.4 AC conductivity

Figure 9 shows the plot of $\sigma_{ac}$ versus angular frequency at various temperatures. The conductivity $\sigma_{ac}$ depends on frequency according to the universal dynamic response given by the phenomenological law:

$$\sigma_{ac} = \sigma_{dc} + A\omega^s$$

where $\sigma_{dc}$ is the DC conductivity, $A$ is a temperature-dependent parameter, and $s$ is an exponent function of temperature and frequency and is related to the degree of correlation among moving ions. It is clear that two different regions are observed from Fig. 9. At the lower frequency ($\omega < 10^5$ rad $s^{-1}$), the DC conductivity shows the existence of a plateau ($\sigma_{dc}$) independent on the frequency. At the higher frequency, the AC conductivity increases in parallel with the increase in frequency and obeying to power law $A\omega^s$. The point at which the change in slope occurs is known as hopping frequency [26], which shifts toward higher-frequency side with the increase in temperature. In the higher-frequency region, the increase in conductivity is due to the hopping of charge carrier in finite clusters.

The temperature dependence of conductivity at various frequencies is displayed in Fig. 10. As seen from the figure, $\sigma_{ac}$ increases linearly with the reciprocal of absolute temperature, indicating that AC conductivity is a thermally activated. Besides, an Arrhenius-type behavior is shown. The value of the activation energy derived from the slope is determined and shown in the inset in Fig. 8.

Such a decrease in activation energy can be attributed to the contribution of the applied frequency to the conduction mechanism. The increment of the applied field frequency enhances the electronic jumps between localized states; hence, the activation energy decreases rapidly with an increase in the applied frequency (higher frequency). The smaller activation energy values and increase in AC conductivity with increasing frequency suggest the hopping to be conduction mechanism [27].

### 3.5 Theory investigation of the correlated barrier hopping (CBH) conduction mechanism

The behavior of the exponent factor $s$ as a function of temperature can be used to determine the origin of the conduction mechanism. Values of the frequency exponent s at different temperature were calculated from the slopes of

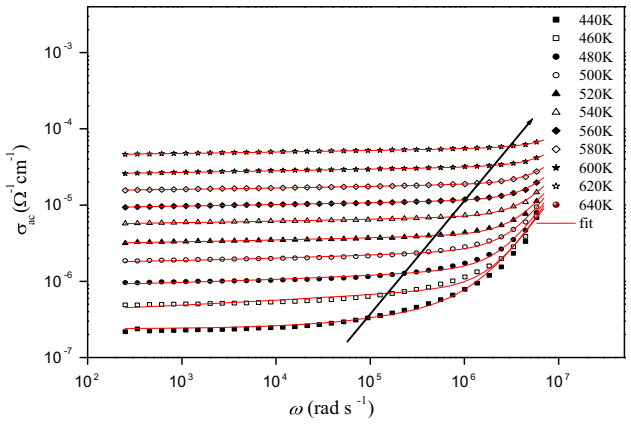


**Fig. 9** AC conductivity as a function of temperature

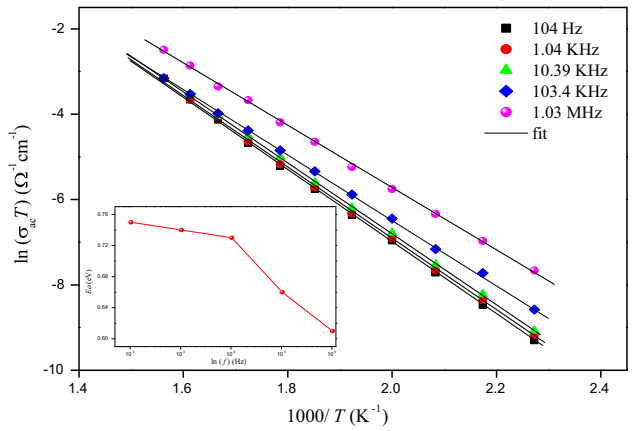


**Fig. 10** Plots of ln $\sigma_{ac}$ vs. 1000/$T$ at different frequencies. The variation of the activation energy with frequency is shown in the inset

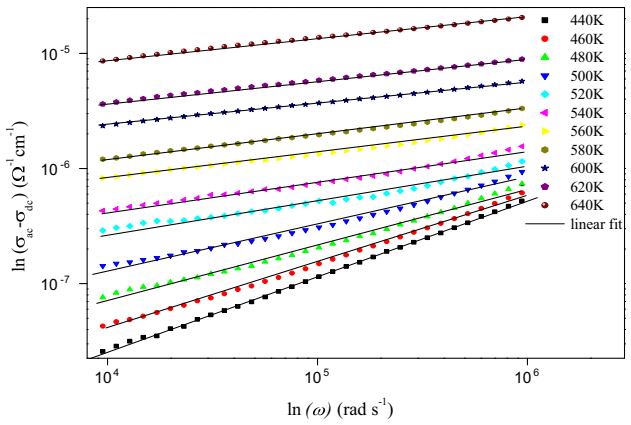


**Fig. 11** Variation logarithm of ($\sigma_{ac}$–$\sigma_{dc}$) versus logarithm of $\omega$

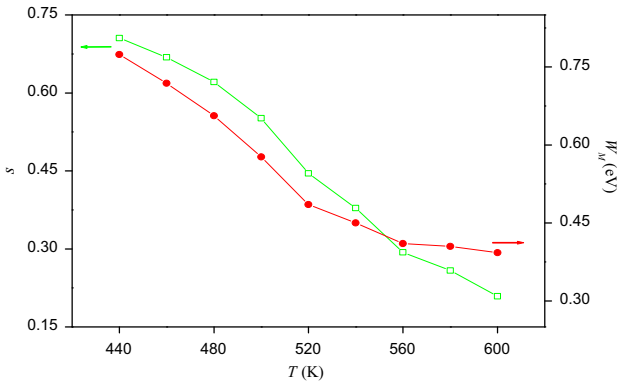


**Fig. 12** Temperature dependence of the exponent s and the binding energy $W_M$

linear part of the relation of log $(\sigma_{ac}^{-}\sigma_{ac}) = f(\omega)$ at the higher-frequency range (Fig. 11). The variation of $s$ with temperature for the investigated compound is shown in Fig. 13. It is observed from this figure that the frequency exponent $s$ decreases with increasing temperature.

To precise the predominant conduction mechanism under AC field for the studied device, different theoretical models have been proposed. In the overlapping-large polaron tunneling (OLPT) conduction mechanism [28], the exponent s decreases with increasing temperature to a minimum value at a certain temperature and then begins to increase with increasing temperature. Therefore, the OLPT conduction mechanism is also not applicable to the obtained results. In the non-overlapping small polaron tunneling (NSPT) conduction mechanism, the exponent s increases with increasing temperature [29]. In the quantum mechanical tunneling (QMT) conduction mechanism [30], the exponent $s$ is almost equal to 0.8 and increases slightly with increasing temperature or is independent of temperature. Therefore, the NSPT and QMT conduction mechanism are also not applicable to the obtained results.

It is clear in Fig. 12 that the value of $s$ decreases with the increase in temperature. Such behavior suggests that the correlated barrier hopping (CBH) conduction mechanism is the predominant conduction mechanism. In CBH model, the conduction occurs via single polaron or bipolaron hopping process over the Coulomb barrier separating two defect centers. The frequency exponent s can be calculated in this model by [31].

$$s = 1 - \frac{6k_B T}{W_M - k_B T \ln(1/\omega\tau_0)} \quad (1)$$

where $k_B$ is the Boltzmann constant, $T$ is the absolute temperature, $W_M$ is the binding energy, ω is the angular frequency, and $\tau_0$ is the characteristic relaxation time, which is in the order of atom vibrational period $\tau_0 = 10^{-13}$ s. For large values of $W_M/k_BT$, the exponent s becomes expressed by [32]:

$$s = 1 - \frac{6K_B T}{W_M} \quad (2)$$

$W_M$ the binding energy is defined as the energy required to move an electron completely from one site to another site. Values of $W_M$ are calculated from Eq. (2) and shown in Fig. 12. $W_M$ decreases with increasing temperature which corresponds to the decrease in the exponent s. So, the number of free carriers which can jump over the barrier will be increased. Consequently, this behavior confirms that the $\sigma_{ac}$ increases with the increasing temperature.

The value of the hopping distance ($R_\omega$) is given by [33]:

$$R_\omega = \frac{q^2}{\pi\varepsilon'\varepsilon_0\left[W_M - k_B T \ln\left(\frac{1}{\omega\tau_0}\right)\right]} \quad (3)$$

where $\varepsilon'$ is the dielectric constant and $\varepsilon_0$ is the permittivity of free space.

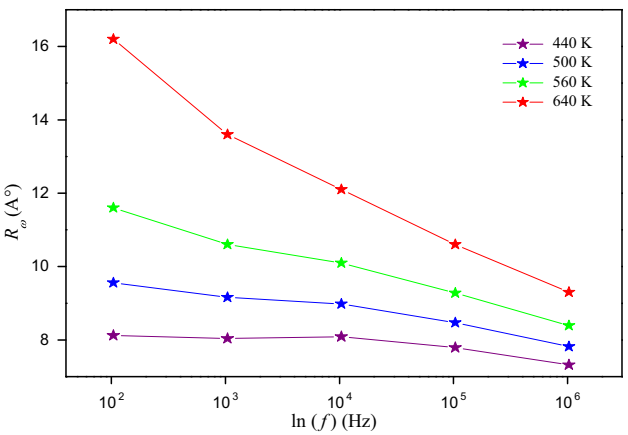


**Fig. 13** Frequency dependence of $R_\omega$(Å) of $AgAlP_2O_7$ at different temperatures

The variation of $R_\omega$ as a function of the frequency at various temperatures is shown in Fig. 13. It can be seen that the hopping distance ($R_\omega$) decreases as the frequency increases. This behavior is in harmony with the increment of the conductivity as the frequency increases.

It is obvious that the hopping distance $R_\omega$ increases with increasing temperature. As a matter of fact, the increasing temperature gives a contribution of thermal energy to polarons, which then will move and facilitate the jump because of the interchain interaction that will occur.

An additional consideration in the crystal structure view point is that this compound induces a significant a polaronic conductor character of the silver sites. As well, the 3D framework is formed with tunnels (Fig. 1), where silver cation resides which is in favor of the conductivity along these tunnels.

## 4 Conclusion

In this work, we have synthesized the $AgAlP_2O_7$ diphosphate compound by the classic ceramic method. From the impedance data, it is concluded that this compound can be modeled by the simple equivalent circuit by R-CPE in series with CPE circuits. An investigation of conductivity properties due to a possible $Ag^+$ ions mobility among structure has been carried out. The AC conductivity for grain response is interpreted using the universal Jonscher's power law. The correlated barrier hopping (CBH) conduction mechanism successfully explained the behavior of temperature conductivity mechanism.

## References


1. E.J. Baran, R.C. Mercader, A. Massaferro, E. Kremer, Spectrochim. Acta A **60**, 1001 (2004)
2. M.E. Hagerman, K.R. Poppelmeyer, Chem. Mater. **7**, 602 (1995)
3. H. Aono, E. Sugimoto, Y. Sadaoka, N. Amanaka, G. Adaki, Solid State Ionics **62**, 309 (1993)
4. J.P. Boilot, G. Collin, P. Colomban, J. Solid State Chem. **73**, 160 (1988)
5. S. Villain, E. Nigrelli, G. Nihoul, Solid State Ionics **116**, 73 (1999)
6. F. Sanz, C. Parada, J.M. Rojo, C. Ruiz-Valero, R. Saez-Puche, J. Solid State Chem. **145**, 604 (1999)
7. C. Delmas, A. Nadini, J.L. Subeyrou, Solid State Ionics **28**, 419 (1988)
8. A. Clearfeld (ed.), *Inorganic ionic exchange materials* (CRC Press, Boca Raton, 1982)
9. S. Arsalane, M. Ziyad, G. Coudurier, J.C. Vedrine, J. Catal. **159**, 162 (1996)
10. Y. Hizhnyi, O. Gomenyuk, S. Nedilko, A. Oliynyk, B. Okhrimenko, V. Bojko, Radiat. Meas. **42**, 719 (2007)
11. Y. Ben Taher, A. Oueslati, M. Gargouri (2014) Ionics. doi: 10.1007/s11581-014-1288-8
12. Y. Ben Taher, R. Hajji A. Oueslati, M. Gargouri (2014) J. Clust. Sci. doi: 10.1007/s10876-014-0812-3
13. S. Nasri, M. Megdiche, M. Gargouri, K. Guidara, Ionics (2013). doi:10.1007/s11581-013-0969-z
14. H.Y.P. Hong, Mater. Res. Bull. **11**, 173 (1976)
15. Goodenough JB (1980) Fast ionic conductors, in UNESCO Course in Materials Science, Erice, Italy
16. A. Daidouh, M.L. Veiga, C.P. Marin, M. Martinez-Ripoll, Acta Crystallogr. C **53**, 167 (1997)
17. S.R.S. Prabaharan, M.S. Michael, S. Radhakrishna, C. Julien, J. Mater. Chem. **7**, 1791 (1997)
18. J.P. Gamaondes, F. d'Yvoire, A. Boulle, C R Acad. Sci. (Paris) **272**, 49 (1971)
19. J. Belkouch, L. Monceaux, E. Bordes, P. Courtine, Mater. Res. Bull. **30**, 149 (1995)
20. B.S. ParajÓn-Costa, R.C. Mercaderb, E.J. Baran, J. Phys. Chem. Solids **74**, 354 (2013)
21. G.T. Stranford, R.A. Condrate Sr, B.C. Cornilsen, J. Mol. Struct. **73**, 231 (1981)
22. A.R. West, D.C. Sinclair, N. Hirose, J. Electroceram. **1**, 65 (1997)
23. C.G. Koops, Phys. Rev. **83**, 121 (1951)
24. H. Rahmouni, M. Nouiri, R. Jemai, N. Kallel, N. Rzigua, A. Selmi, K. Khirouni, S. Alaya, J. Magn. Magn. Mater. **316**, 23 (2007)
25. Moti Ram, Solid State Sci. **12**, 350 (2010)
26. K. Srinivas, P. Sarah, S.V. Suryanarayana, Bull. Mater. Sci. **26**, 247 (2003)
27. Okutan M, Basaran E, Bakan HI, Yakuphanoglu F (2005) J Phys B 364:300
28. A.R. Long, Adv. Phys. **31**, 553 (1982)
29. A. Ghosh, Phys. Rev. B **42**, 5665 (1990)
30. M. Pollak, Phil. Mag. **23**, 519 (1971)
31. V. Chithambaram, S. Jerome Das, S. Krishnan, J. Alloys Compd. **509**, 4543 (2011)
32. K.H. Mahmoud, F.M. Abdel-Rahim, K. Atef, Y.B. Saddeek, Curr. Appl. Phys. **11**, 55 (2011)
33. I.A. Niel, Proc SPIE **237**, 422 (1980)